

Three-phase model for the reversible lithiation/delithiation of SnO anodes in Li-ion batteries

Andreas Pedersen,^{1,*} Petr A. Khomyakov,¹ and Mathieu Luisier¹

¹*Integrated Systems Laboratory, Department of
Electrical Engineering and Information Technology,
ETH Zurich, Gloriastrasse 35, 8092 Zurich, Switzerland*

(Dated: December 3, 2024)

Abstract

Using first-principles calculations, we propose a microscopic model to explain the reversible lithiation/delithiation of tin-oxide anodes in lithium-ion batteries. When the irreversible regime ends, the anode grains consist of layers of Li-oxide separated by Sn bilayers. During the following reversible lithiation, the Li-oxide undergoes two phase transformations that give rise to a Li-enrichment of the oxide and the formation of a SnLi composite. The anode grain structure stays layered and ordered with an effective theoretical reversible capacity of 4.5 Li per Sn atom. The predicted anode volume expansion and voltage profile agree well with experiments, contrary to existing models.

Keywords: Tin-oxide, Anode, Reversible, Lithiation, Density Functional Theory

Tin-based compounds are promising candidates to replace graphite as the anode material in lithium-ion batteries (LIBs) [1]. Having a maximum capacity of 4.4 Li per Sn atom ($\text{Li}_{22}\text{Sn}_5$) [2], Sn alloys outperform the theoretical gravimetric limit of graphite by a factor larger than two [3]. The interest for Sn-based material systems was originally sparked by the pioneering work of Idota *et al.* [4] who showed that using an amorphous tin composite oxide as the anode of a LIB cell improves the performance of the battery both in terms of capacity and cycleability.

To better understand the behavior of Sn-based materials upon lithiation and delithiation, Courtney and Dahn [5] conducted a series of experiments on various Sn-oxides. They found that all the oxides initially undergo an irreversible Li uptake followed by a regime where Li insertion and extraction exhibit a reversible behavior. Using their experimental findings, Courtney and Dahn developed an empirical model where it is assumed that an amorphous Li-oxide matrix forms as the initial Li ions enter into the pristine SnO sample. The O atoms are captured by Li, which offers stronger bonds as compared to Sn. At the same time, the Sn atoms agglomerate into clusters embedded in the emerging Li-oxide matrix. The proposed Sn clustering model is based on the experimental observation of Sn signatures in X-ray diffraction measurements on the lithiated oxide materials [5]. Note that the aforementioned structural changes of SnO take place during the initial irreversible Li uptake. As the lithiation continues, Sn is assumed to become a SnLi_x alloy, where x is the number of Li atoms per Sn. This alloy provides the reversible storage medium for Li. The model proposed by Courtney and Dahn has served as a reference for interpreting lithiation/delithiation of Li-ion battery cells with SnO-based anode electrodes. While the formation of a Li-oxide has been confirmed by several other groups [6–8], the occurrence of Sn clusters is being questioned since it cannot explain the presence of all the observed bond types [7–10]. We adapt this model to LiOSn anodes by assuming that the Sn clusters behave similarly to bulk SnLi_x when exposed to Li. This will be referred to as the *cluster model*.

In a recent experiment, Ebner and co-workers carefully determined the voltage profile resulting from the lithiation of SnO as well as the volume expansion taking place during the first Li charge/discharge cycle [11]. They also found that fracturing tends to occur at grain boundaries in SnO, which is difficult to explain when one assumes that a homogenous isotropic amorphous Li-oxide matrix with separated Sn clusters forms. Since Li-oxide is a good insulator, the assumption of fully segregated Sn clusters further makes it difficult to

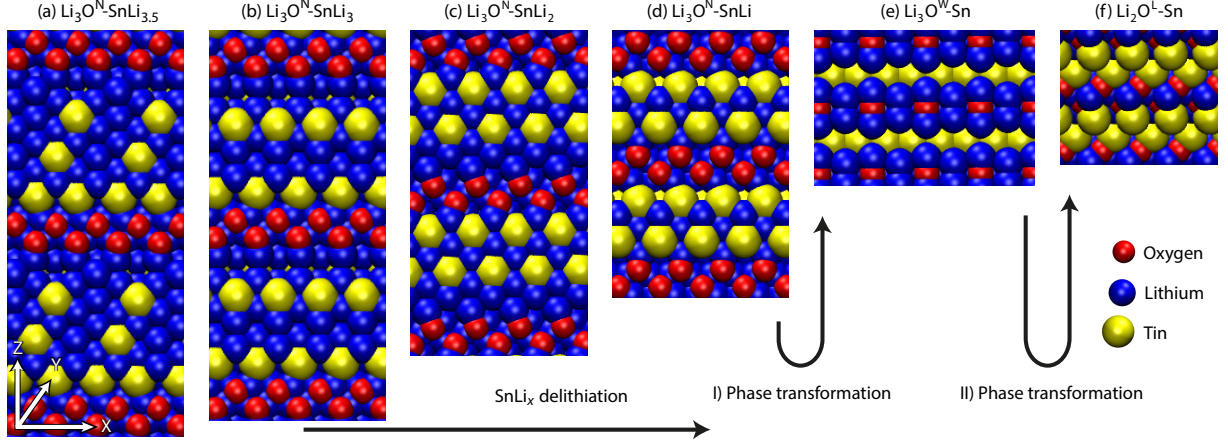


FIG. 1. $\text{Li}_y\text{O-SnLi}_x$ structural configurations for x (y) decreasing from 3.5 to 0 (from 3 to 2) and undergoing two phase transformations. Blue, red, and yellow sphere correspond to the Li, O, and Sn atom, respectively. Initially, 2.5 Li-layers are released, causing Li depletion of SnLi_x from $x=3.5$ to 1, as shown in insets (a)-(d). The remaining Li layer in the SnLi composite structure is freed as the Li-oxide changes its phase from $\text{Li}_3\text{O}^{\text{N}}$ to $\text{Li}_3\text{O}^{\text{W}}$, inset (e). Another phase transformation occurs upon further Li extraction, bringing the Li-rich oxide to its irreversible $\text{Li}_2\text{O}^{\text{L}}$ phase, inset (f).

conceive how electrons can be efficiently supplied to the conductive SnLi_x clusters, unless they are well interconnected. Note that this connectivity should be maintained for any cluster volume, which varies by more than a factor of three.

In this Letter, we propose a microscopic model based on a first-principles study for the reversible lithiation/delithiation of tin monoxide that goes beyond the limitations of the empirical model by Courtney and Dahn [5]. According to our recent *ab-initio* calculations of the irreversible Li-uptake, a fully Li-depleted anode consists of layered Li-oxide separated by Sn bilayers [12]. Starting from this configuration, we show that the Li-oxide undergoes two phase transformations as the Li concentration increases, which leads to the formation of a Li-rich, layered, and ordered Li-oxide (Li_3O). After that additional Li atoms are solely accommodated in the Sn layer whose capacity is 3.5 Li per Sn atom. The final structure therefore contains 6.5 Li per Sn atom, but the effective total *reversible capacity* is limited to 4.5 Li per Sn atom because two Li layers are strongly bound to the O atoms. By applying this *three-phase model* we are able to reproduce the experimentally determined volume expansion as well as the qualitative behavior of the measured voltage profile. The simulated LiOSn

structures also exhibit a good electron conductance because of their highly-conductive SnLi layers.

Our first-principles calculations rely on a density-functional plane-wave pseudo-potential method within the framework of the generalized gradient approximation (GGA-PBE) [13] and the projector augmented wave (PAW) formalism [14], as implemented in the VASP code [15, 16]. The equilibrium LiOSn structures are obtained by total energy minimizations of a $8 \times 8 \times 1$ SnO supercell structure (64 Sn and 64 O atoms) with a Li content ranging from 128 to 448 atoms. The supercell Brillouin zone is sampled with a $2 \times 2 \times 2$ k-point grid. The plane-wave kinetic energy cut-off is set at 500 eV. The total energy and forces are converged to at least 10^{-8} eV and 10^{-3} eV/Å, respectively. For a better sampling of the configuration space, we also perform molecular dynamics (MD) simulations with a high temperature ($T < 10^3$ K) Nose-Hover thermostat. This allows for structural rearrangements following transitions between nearby local minima of the LiOSn potential energy surface. The LiOSn structural configurations obtained from the MD trajectory are inspected by the eye, and atoms are moved if they appear not to conform a dominant pattern. Atom relaxation as well as relaxation of the supercell shape and volume are subsequently done for the refined structures.

We now describe in detail the entire process of the anode lithiation as given by the proposed three-phase model. The starting configuration corresponds to the anode grain structure, in which the irreversible uptake of Li is fully complete, and the Li-oxide layers are separated by Sn bilayers, as shown in Fig. 1(f) and in Ref. [12]. Layers or half-layers of Li are inserted into the structure as long as the relative binding energy for Li remains negative

$$E_b = \frac{E_L - (E_{L-1} + N_L \cdot E_{\text{Li}})}{N_L}, \quad (1)$$

where E_b is the average relative binding energy of a single Li atom; E_L is the total energy of the anode structure with L layers of Li; E_{Li} is the cohesive energy of a Li atom in a bulk environment, and N_L is the number of Li atoms in a single Li layer. Structures fulfilling the requirement $E_b < 0$ in Eq. (1) have been determined for Li concentrations up to $L = 6.5$. This Li content corresponds to a fully lithiated SnO sample. For $L \geq 7$ the additional Li atoms are located in the LiOSn structure within an environment similar to bulk Li and have a comparable binding energy so that $E_b > 0$. This indicates that eventual overcharging is likely to result in the formation of domains with bulk Li, which, in the best case scenario,

just act as passive spectators. In other words, having any extra Li atoms in the fully-loaded anode structure does not increase the battery capacity since these Li atoms will not be released by the layered anode upon normal discharging conditions.

Figure 1 shows all the structural configurations obtained during the lithiation process described in the previous paragraph. As the Li load increases, three different phases can be identified, which are separated by two phase transformations of the Li-oxide. The first phase, $\text{Li}_2\text{O}^{\text{L}}$, corresponds to the fully Li-depleted configuration in Fig. 1(f). The label L underlines its *layered* structure in which the Sn metallic bilayers surround the insulating Li-poor oxide layers. A second phase, $\text{Li}_3\text{O}^{\text{W}}$, as shown in Fig. 1(e), appears upon insertion of the first reversible Li layer. The XY cross section of this oxide layer expands so that the label W stands for its *wider* cross section area. Note that no substantial change of the supercell size occurs in the Z direction though the Sn bilayer transforms into a monolayer structure. Four structural configurations of a third Li-oxide phase, $\text{Li}_3\text{O}^{\text{N}}$, are shown in Figs. 1(a)-(d). This oxide results from a phase transformation where the number of Li atoms remains unchanged and the Li-rich oxide regains a narrow XY cross section. The label N refers to its *narrower* cross section area. Hereafter, the inserted Li atoms form a SnLi_x layered composite structure that is accompanied by a strong expansion of the corresponding supercell in the Z direction. The layered composite can accommodate a maximum of 3.5 Li per Sn atom. The fully-loaded structural configuration is given in Fig. 1(a). From Fig. 1 it is also apparent that the three-phase model offers an explanation for the “unusual” bond types through the presence of Sn-Sn, Sn-Li, Sn-O, and Li-O bonds in the layered anode grains.

To describe the delithiation process, one has to determine how the atoms are extracted from the anode. In the present study, we only focus on the first reversible lithiation/delithiation cycle under the assumption that the initial and irreversible transformation from Sn- to Li-oxide has already taken place. To validate the three-phase model against the experimental data in Ref. 11, we computed the volume expansion of the $\text{Li}_y\text{O-SnLi}_x$ anode with respect to the volume of pristine SnO upon Li-extraction, as reported in Fig. 2. The volume expansion is defined as

$$\Delta V = \frac{V - V_{\text{SnO}}}{V_{\text{SnO}}} \cdot 100\%, \quad (2)$$

where V is the volume of the $\text{Li}_y\text{O-SnLi}_x$ supercell at a given Li concentration (x and y), and V_{SnO} is the volume of a pristine SnO structure with the same number of Sn atoms as in

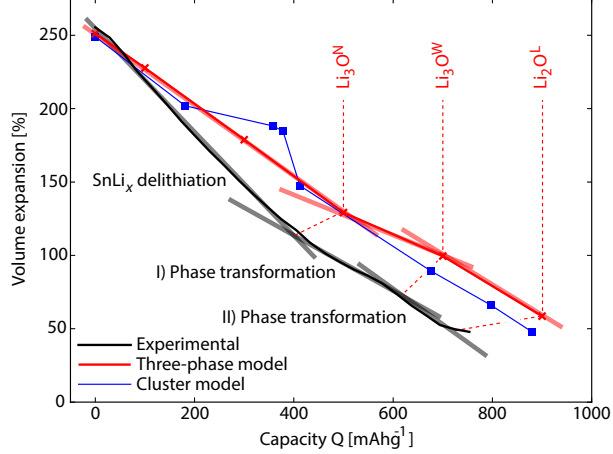


FIG. 2. Volume expansion of the LiOSn anode during delithiation. The volume expansion is defined with respect to the volume of pristine SnO. Red crosses and filled blue squares refer to the numerical data computed with the three-phase model and the cluster model, respectively. The black, blue, and red solid lines correspond to the experimental data [11], the cluster, and the proposed three-phase model, respectively. The solid lines only serve as a guide to the eye. Three volume expansion regimes can be identified. They are delimited by the three gray straight lines. The delithiation process evolves as follows: (i) Li is released from the SnLi_x composite structure sandwiched between $\text{Li}_3\text{O}^{\text{N}}$ layers, (ii) the Li-oxide transforms into $\text{Li}_3\text{O}^{\text{W}}$ separated by Sn monolayers, and (iii) a second transformation into a layered $\text{Li}_2\text{O}^{\text{L}}$ oxide with Sn bilayers in-between occurs.

the corresponding LiOSn supercell.

The three volume expansion regimes, which can be clearly identified in Fig. 2, correspond to the three Li-oxide phases shown in Fig. 1. At first, Li atoms are released from the SnLi_x composite structure, which is situated in-between $\text{Li}_3\text{O}^{\text{N}}$ layers. This causes a constant volume reduction imposed by the supercell contraction in the Z direction, perpendicular to the XY cross section. While SnLi_x becomes fully Li-depleted, the Li-rich oxide undergoes a phase transformation ($\text{N} \rightarrow \text{W}$) that slows down the volume reduction. Though the atom rearrangement in the anode grain structure is rather drastic, the corresponding volume reduction is quite moderate because of the significant XY cross section expansion, which compensates for the supercell contraction in the Z direction. Finally, further delithiation extracts the remaining Li atoms that are loosely-bound in the oxide, giving rise to another transformation ($\text{W} \rightarrow \text{L}$). This brings back the anode structure into its original $\text{Li}_2\text{O}^{\text{L}}$ phase

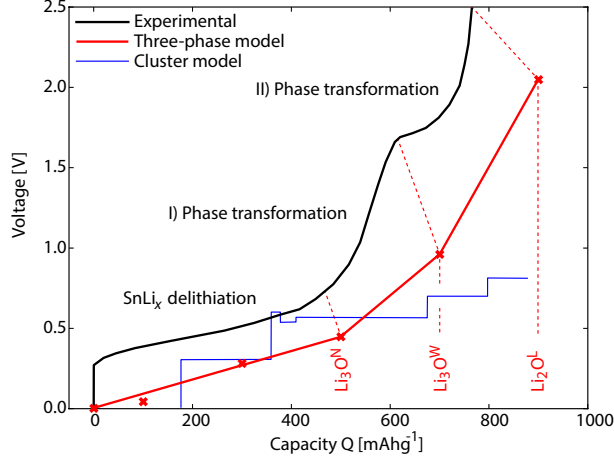


FIG. 3. Voltage profile of the LiOSn anode structure during delithiation. The voltage is defined with respect to a Li counter electrode (zero-voltage reference). The same plotting conventions as in Fig. 2 are used. Note that the data points for a bulk SnLi_x alloy are shifted along the X-axis to coincide with the corresponding points in Fig. 2. The first step-like segment of the voltage profile refers to the SnLi_x delithiation. The two segments with a steeper slope correlate with a phase transformation and a Li-depletion of the Li-oxide, first from $\text{Li}_3\text{O}^{\text{N}}$ to $\text{Li}_3\text{O}^{\text{W}}$, followed by the phase transformation to $\text{Li}_2\text{O}^{\text{L}}$.

with a narrow cross section, as depicted in Fig. 1(f). This final transformation induces a strong volume reduction. Figure 2 shows that the volume expansion, as predicted by the three-phase model, is in a good agreement with the volume change measured in Ref. 11. The strong dependence between the anode grain volume and the Li-concentration is noteworthy. It may give rise to a deterioration of the layered structure during battery operation if the Li concentration is inhomogeneous over the anode volume. This could explain why Li-oxide has been classified as amorphous in LiOSn anodes [5]. It also resolves why fracturing tends to occur at grain boundaries. These fractures take place to relieve accumulated strain in the regions where crystal grains of different orientation and shape touch each other upon volume expansion.

To further validate the three-phase model, we calculated the voltage profile of the LiOSn anode during delithiation, as shown in Fig. 3. A previous work on SnLi alloys [17] demonstrated that the voltage profile, which is determined by the change of the Gibbs free energy, can be obtained by calculating the internal energy change only, while the entropy and volume terms can be safely neglected. We adopt a similar approach to compute the voltage

profile during delithiation

$$\Delta U = \frac{(E_{6.5-\Gamma} + \Gamma \cdot N_L \cdot E_{\text{Li}}) - E_{6.5}}{\Gamma \cdot N_L \cdot e}, \quad (3)$$

where ΔU is the voltage change relative to the fully-lithiated anode structure with the total energy $E_{6.5}$; $E_{6.5-\Gamma}$ is the total energy of an anode structure with Γ Li layers removed; N_L is the number of Li atoms in a single Li layer, and e is the elementary charge of an electron.

Figure 3 shows that a rather moderate increase of the voltage takes place as the Li atoms are released from the SnLi_x composite structure during the first stage of delithiation ($0 < Q < 500 \text{ mAhg}^{-1}$). A steep voltage increase then occurs as the SnLi composite is depleted of Li atoms and the Li-rich oxide undergoes a phase transformation ($500 < Q < 700 \text{ mAhg}^{-1}$). Finally, the further extraction of Li atoms from the Li-rich oxide ($700 < Q < 900 \text{ mAhg}^{-1}$) increases the voltage up to its maximum value of 2.05 eV for the fully Li-depleted anode structure (Fig. 1(f)). One can see in Fig. 3 that the three-phase model reproduces the experimentally observed voltage profile qualitatively well [5–7, 11]. Figure 3 also suggests that the Sn cluster model is not applicable for the LiOSn anode grain.

We notice that the voltage profile given by the three-phase model misses the onset of 0.3 V that is present in the experimental data at the capacity $Q = 0$. This can be explained by the fact that the computed voltage is determined from an average change in the total energy of the anode, as given in Eq. 3, whereas eventual activation energy barriers of the Li atom diffusion process upon delithiation have not been accounted for. As a first approximation, the onset voltage can be estimated in the following way. When removing a single Li atom from the anode structure, it appears that the Li atoms residing at the interface between the Li-oxide and the composite layers have the weakest bonds. This holds true for all the structures, except the one with a fully Li-loaded anode (Fig. 1(f)) in which the least bound Li is in the SnLi composite layer. The energy required to extract this Li atom from the composite layered structure is 0.16 eV i.e., 0.16 V can be considered as the lower bound for the onset voltage at the capacity $Q = 0$.

The anode grain structure, as given by the three-phase model, has been assumed to be a good electrical conductor during the entire lithiation/delithiation cycle. This means that all the layered structures in Figs. 1(a)-(f) should have a high in-plane electron conductance comparable to that of bulk β -Sn and Li. To confirm this hypothesis, we have calculated the band structure of the Li-oxide and SnLi composite layers, which reveals that the oxide

layer is an insulator with a sizable band gap, whereas the SnLi composite layer is metallic and provides conducting channels for electron transport. First-principles calculations of the ballistic electron transport through the SnLi composite layers in Fig. 1 explicitly show that the in-plane electron conductance is comparable to that of bulk β -Sn and Li calculated using the same approach. Hence, the proposed anode structure is a good conductor. This finding is consistent with experimental observations. Details about the conductance calculations will be published elsewhere [18].

We have done first-principles, density-functional theory calculations to understand the reversible lithiation/delithiation of SnO anodes in Li-ion batteries at the microscopic level. Based on these atomistic simulations, we developed a three-phase model that consistently explains how the structural and electronic properties of a SnO-based anode (phase transformation, volume expansion, voltage profile, and electron conductance) evolve during the initial lithiation/delithiation cycle. This microscopic model goes significantly beyond existing theories such as the widely used empirical model by Courtney and Dahn [5]. It predicts that the effective reversible capacity of the SnO-based Li-ion battery can reach up to 4.5 Li per Sn atom, which is slightly higher than the theoretical capacity limit for a SnLi_x -alloy [2]. It sheds light onto the puzzling experimental observation of “unusual” bonds, which can be explained by a high ratio of Sn-Sn, Sn-Li, Sn-O, and Li-O bonds in the layered LiOSn structure. It also offers an explanation for the deterioration and amorphization of the LiOSn structure, which will be caused by inhomogeneities in the Li concentration. Finally, the three-phase model might be applicable to other metal-oxide anodes that show a similar voltage profile upon lithiation [19].

This research is funded by the EU Commission (the ERC starting grant: E-MOBILE). The computer simulations are done at the Swiss National Supercomputer Center (project: s503). The authors thank Martin Ebner for helpful discussions.

* andped10@gmail.com

[1] M. N. Obrovac, L. Christensen, D. B. Le, and J. R. Dahn, *Journal of The Electrochemical Society* **154**, A849 (2007).

[2] B. A. Boukamp, G. C. Lesh, and R. A. Huggins, *Journal of The Electrochemical Society* **128**,

- 725 (1981).
- [3] C.-M. Park, J.-H. Kim, H. Kim, and H.-J. Sohn, *Chemical Society Reviews* **39**, 3115 (2010).
 - [4] Y. Idota, *Science* **276**, 1395 (1997).
 - [5] I. A. Courtney and J. R. Dahn, *Journal of The Electrochemical Society* **144**, 2045 (1997).
 - [6] J. Chouvin, J. Olivier-Fourcade, J. C. Jumas, B. Simon, P. H. Biensan, F. Madrigal, J. L. Tirado, and C. P. Vicente, *Journal of Electroanalytical Chemistry* **494**, 136 (2000).
 - [7] Y. Wang, J. Sakamoto, S. Kostov, A. N. Mansour, M. L. denBoer, S. G. Greenbaum, C. K. Huang, and S. Surampudi, *Journal of Power Sources* **89**, 232 (2000).
 - [8] I. Sandu, T. Brousse, D. M. Schleich, and M. Danot, *Journal of Solid State Chemistry* **177**, 4332 (2004).
 - [9] I. A. Courtney, R. A. Dunlap, and J. R. Dahn, *Electrochimica Acta* **45**, 51 (1999).
 - [10] I. Sandu, T. Brousse, D. M. Schleich, and M. Danot, *Journal of Solid State Chemistry* **179**, 476 (2006).
 - [11] M. Ebner, F. Marone, M. Stampanoni, and V. Wood, *Science* **342**, 716 (2013).
 - [12] A. Pedersen and M. Luisier, *ACS Applied Materials & Interfaces* **6**, 22257 (2014).
 - [13] J. P. Perdew, K. Burke, and M. Ernzerhof, *Physical Review Letters* **77**, 3865 (1996).
 - [14] P. E. Blöchl, *Physical Review B* **50**, 17953 (1994).
 - [15] G. Kresse and J. Furthmuller, *Physical Review B* **54**, 11169 (1996).
 - [16] G. Kresse and J. Furthmuller, *Computational Materials Science* **6**, 15 (1996).
 - [17] I. A. Courtney, J. S. Tse, O. Mao, J. Hafner, and J. R. Dahn, *Physical Review B* **58**, 15583 (1998).
 - [18] P. A. Khomyakov, A. Pedersen, and M. Luisier, (unpublished).
 - [19] P. Poizot, S. Laruelle, S. Grugeon, and L. Dupont, *Nature* **407**, 496 (2000).